



## Photocatalytic, anti-microbial, antioxidant and cytotoxic activity of electrochemically synthesized ZnO-TiO<sub>2</sub> nanostructures

Jenice Jean Goveas<sup>1</sup>, Ajay Sathaynarayanrao Khandagale<sup>2</sup>, Sandhya Shetty<sup>3</sup> and Richard Adolf Gonsalves<sup>1\*</sup>

<sup>1</sup>Department of Chemistry, St Aloysius College (Autonomous), Mangalore-575003, India

<sup>2</sup>College of Fisheries Mangalore-575003, India

<sup>3</sup>St Agnes Centre for Post Graduate Studies and Research, Mangalore-575002, India  
richieag@yahoo.com

Available online at: [www.isca.in](http://www.isca.in), [www.isca.me](http://www.isca.me)

Received 26<sup>th</sup> November 2019, revised 2<sup>nd</sup> March 2020, accepted 10<sup>th</sup> April 2020

### Abstract

Mixed metal oxide nanoparticles (NPs) of ZnO-TiO<sub>2</sub> (ZTiO) were synthesized using a simplistic two-step electrochemical-thermal route in the presence and absence of three surfactants: Cetyltrimethyl ammonium bromide (Cetrimide), Sodium dodecyl sulphate (SDS) and polyethylene glycol (PEG). This investigation intended to assess the possible applicability of these nanocomposites for degradation of 2 organic aqueous dyes-methylene Blue (MB) and Eriochrome Black-T (EBT). The potential application of ZTiO as antimicrobial agents was also investigated using disc diffusion technique against the Gram-negative bacteria, *Pseudomonas aeruginosa*, *Escherichia coli*, *Klebsiella pneumoniae* and the Gram-positive *Staphylococcus aureus*. Antioxidant property of the NPs was established by DPPH radical scavenging technique. The particles show a considerably high bacteriostatic effect towards all the pathogens tested. ZTiO also showed significant cytotoxicity to HeLa breast cancer cells. This proves that the electrochemical synthetic route with its low cost and high efficiency is a competent technique for the large-scale synthesis of heterometal oxide photocatalysts which could potentially be used as effective therapeutic agents.

**Keywords:** ZnO-TiO<sub>2</sub>, photocatalyst, nanocomposites, cytotoxicity, antimicrobial, antioxidant.

### Introduction

The past few decades have witnessed an escalating demand for metal oxide nanostructured materials which can offer solutions to various problems of the environment, electronics and biology<sup>1</sup>. Heterogeneous photocatalysis is an attractive and efficient technology for bringing about photodegradation in organic wastes-particularly dyes present in effluent water. It is alluring and beneficial as it brings about complete mineralisation of these compounds<sup>2,3</sup> with the added advantage of affordability, ease of production, and specificity<sup>4,5</sup>. Nanomaterials possess relatively large turn-over capacities, retrievability and recyclability<sup>6</sup>. Effectual charge separation which prolongs the life of the generated charge carriers is favourable for photooxidation and mineralization<sup>7</sup>. This has been achieved by coupling semiconductors possessing different corresponding conduction and valence band energy levels<sup>8</sup>.

Among the many semiconductors, ZnO and TiO<sub>2</sub> have established themselves as promising photocatalysts owing to interesting optical and electrical properties, economic viability, stability, and easy accessibility<sup>9</sup>. The composite exhibits greater photocatalytic activity relative to the pure parent metal oxides. This may be accredited to an extended range of light absorptivity in addition to effective transfer of charge between ZnO and TiO<sub>2</sub><sup>10</sup>. Photocatalysis using such a hybrid ZnO-TiO<sub>2</sub> semiconductor composite is a relatively novel method

which includes fabricating the semiconductor metal oxidenano structures possessing tunable physico-chemical properties.

Nano structured biomaterials have conspicuous features one of which is the ability to circulate in the blood stream taking advantage of their small size giving them access to specific cells.<sup>11</sup> Various reports reveal how antibiotics disturb the typical bacterial flora of the digestive tract resulting in threat of multidrug resistance.<sup>12</sup> The emphasis for developing novel biocides possessing good bactericidal properties which do not generate resistance gains prominence. One of the functional applications of antibacterial bioactivity is in the food packaging industry in which nanoparticles (NPs) are employed as antibacterial agents to resist foodborne ailments. These NPs are released onto the food surface and when they come in contact with the food borne pathogens, they cause bacterial death or inhibition<sup>13</sup>.

Nanocomposites present wide applications in medicine, biotechnology and effluent water treatment owing to their modifiable properties, high stability and nano size<sup>14,15</sup>. However, most methods espoused for their synthesis utilize expensive substrates, rigorous techniques, sophisticated equipment and complicated experiments in difficult conditions<sup>16</sup>. In this work, the authors present an analysis of the antimicrobial, photocatalytic, antioxidant and cytotoxic activity of hetero metal oxide nanoparticles of ZnO-TiO<sub>2</sub> synthesized

using a facile electrochemical process in the presence and absence of surfactants.

## Materials and Methods

Superior quality zinc plates (99.99%) have been used as electrodes. Analytical grade reagents were procured from Sisco Research laboratories, Mumbai. Electrolysis was performed at a steady voltage of 12V using a PS 618 model potentiostat. Filtration was carried using Whatman No. 41 filter paper. Streptomycin 10mcg/disc were bought from Hi-Media. Human promyelocytic leukemia (HL-60) cell line from NCCS-Pune were maintained under ideal conditions. RPMI-1640 medium was enhanced using Foetal Bovine Serum (10% FBS) and stored at 4°C for 30 days.

**Synthesis of nanocomposites:** Mixed metal oxide NPs were fabricated by a standard electrochemical technique.<sup>17</sup> Priorly activated zinc plates were employed for electrolysis. Activation was achieved by dipping in dil. HCl for 30 seconds and then rinsing in pure (millipore) water. A 400mL solution of Na<sub>2</sub>Ti<sub>3</sub>O<sub>7</sub> was taken in an undivided rectangular pyrex vessel which contained 0.01 moles of NaHCO<sub>3</sub> for conductance. pH was maintained steady at 10 using NH<sub>4</sub>OH/NH<sub>4</sub>Cl buffer. Pure Zn plates acted as both cathode and anode. Potentiostatic conditions (12V) were maintained for one hour of electrolysis with continual magnetic agitation at 500rpm. The obtained white ZTiO powder was filtered followed by calcination for one hour at different temperatures. Mixed metal oxide NPs were also fabricated by adding 3 synthetic surfactants (cetrimide, SDS and PEG) to the electrolytic bath in amounts just above their critical micellar concentrations.

**Assessment of photocatalytic activity of MB and EBT:** Photocatalysis was carried inside a 150×75 mm pyrex reactor under Ultraviolet light using a mercury high-pressure vapor lamp (flux =5.8×10<sup>-6</sup>mol photons s<sup>-1</sup>). Temperature was maintained at 30±2°C. To prevent fluctuation of the input light intensity, the lamp was connected to a capacitor and supply ballast in series. Water circulation through the quartz tube avoided excess heating. The reaction suspension included the catalytic load in which 0.1g of ZTiO in 100mL MB/EBT (5,10, 25ppm) solution was taken. The suspension was kept in the dark for 2 hours prior to illumination and magnetically stirred to attain uniform absorption-desorption equilibrium. Absorbance values of MB and EBT were recorded at 660nm and 568nm respectively. Experiments were performed in triplicate. Relative error observed was lower than ±3.0%. The results for the optimized ZTiO photocatalyst are presented in comparison to the standard photocatalyst Degussa P25 TiO<sub>2</sub>.

**Antimicrobial property:** Antibacterial property was studied using agar well diffusion method<sup>18</sup> against Gram-negative bacteria *K. pneumoniae*- NCIM2719, *E. coli*- NCIM5051, *P. aeruginosa*- NCIM2242 and Gram-positive bacteria *S. aureus* - NCIM5022. Spread plate technique was employed for the

preparation of sterile nutrient agar plates. A 0.7mm sterile blotting paper disc was saturated with 30μL of NPs, dried and added over the top layer of the seeded nutrient agar plate. 100μL of the inoculums (1.0×10<sup>8</sup> Cfu/mL) was introduced into the agar plate. The synthesised ZTiO nanoparticles were dissolved in 20% DMSO solvents under sterile conditions. Streptomycin 10 mcg/disc was employed as the positive control. DMSO soaked disc was the negative control. Incubation of the plates at 37°C was carried out for 24 hours after which the zones of inhibition were measured in triplicates.

**Antioxidant property: DPPH radical scavenging:** Correctness and repeatability makes the DPPH method a preferred choice for researchers for the assessment of the NPs inhibition potential towards generation of radicals<sup>19</sup>. Standard ascorbic acid (0.1 mg/mL) solution was taken in different test tubes along with diluted NPs (0.1mg-1.0mg/mL) and made up to 1.0mL using methanol. 3.0mL of DPPH (0.1M) was added. It was thoroughly mixed in a vortex machine. This mixture was left aside away from light for 30 mins. Absorbance readings at 517nm wavelength were taken. Assessment of radical scavenging ability was done and expressed as percentage with the help of the given equation.

$$\text{Inhibition \%} = \frac{A_{(\text{control})} - A_{\text{test}}}{A_{(\text{control})}} \times 100 \quad (1)$$

**Reducing power assay:** Reducing power was appropriately determined by employing a standard technique<sup>20</sup>. In different incubation tubes, Standard solution (0.1mg/mL) along with diluted solution of NPs (1.0mg/mL) were analysed. 2mL of a pH 6.6 phosphate buffer was added to reaction batch along with 2.5mL of 1% solution of potassium ferricyanide. The tubes were then incubated suitably at 50°C for 20 mins. 2.5mL solution of 10% CCl<sub>3</sub>COOH was added along with 0.5mL of FeCl<sub>3</sub> solution (0.1%) and 2.5mL of distilled water and thoroughly mixed using a vortex mixer. The changed absorbance was monitored with time using a UV spectrophotometer (λ<sub>max</sub> = 700nm).

**Cytotoxic activity:** Assessment of cytotoxic/anticancer activity on human leukemic cancer cells was achieved by MTT assay, to analyse the cytotoxic activity of different ZTiO nano powder on different cell lines<sup>21</sup>. 96 well plate containing 100μL culture medium was seeded with 5×10<sup>4</sup> cells per well. It was kept for incubation at 37 °C for 24 hours along with 5.0% CO<sub>2</sub>. These cells were further treated with ZTiO nano powder of varying (25,50,75,100,125,150,175 and 200μg/mL for both cells) concentration and further set aside for 24-72 hours incubation. Subsequently, 10μL MTT solution (1.0mg/mL) prepared in Phosphate buffered saline (PBS). On addition to each well a formazan product was formed. For quantification a Bio-Rad microplate reader was used and the cell proliferation was assessed by calculating IC<sub>50</sub> values.

**Catalyst characterization:** General morphology, structure, crystallite size etc of the NPs was understood from its Powder

X-ray diffraction (XRD) spectrum along with their compositional analysis. Rigaku Miniflex (600) X-ray diffractometer with Cu-K $\alpha$  (1.5406Å) radiation was employed and recording was done in 2 $\theta$  range of 10°- 90° at 1° min<sup>-1</sup>s can rate. Using Bruker Alpha-P spectrometer, FTIR spectrum of the ZTiO NPs was obtained. Shimadzu UV-1800 was used for recording of UV-Vis Absorption spectrum. Surface morphology assessment was performed by transmission and scanning electron microscopy by using JEOL (2000) FX-II Transmission electron microscope and Carl Zeiss EVO 18 scanning electron microscope respectively. Computation of the structure was done with the help of PANalytical software X'Pert High score.

## Results and discussion

**Compositional analysis of ZTiO heterometal oxide nanostructures:** The XRD patterns of ZnO-TiO<sub>2</sub> NPs is illustrated in Figure-1(a). As observed the patterns display crystalline nature for ZTiO reveals the growth of ZnO crystals on TiO<sub>2</sub> nanoparticles. XRD patterns reveal their polycrystalline nature with mixed hexagonal, orthorhombic and tetragonal phases. TiO<sub>2</sub> too possesses three typical phases which include brookite, anatase and rutile. Anatase and rutile display crystalline tetragonal structure whereas Brookite have crystalline orthorhombic structure. A reaction between ZnO and TiO<sub>2</sub> to form spinel Zn<sub>2</sub>TiO<sub>4</sub> is observed as also seen in earlier reports<sup>22, 23</sup>.

The peaks which appears at 2 $\theta$  = 17.7° and 29.13° corresponds to Zn<sub>2</sub>TiO<sub>4</sub> (101) and (112) planes (JCPDS card no. 19-1483).<sup>24</sup> The chief peaks at 2 $\theta$  include those at 34.32° and 35.94° correspond to the (002), and (101) planes of hexagonal Zincate (JCPDS card No. 36-1451). The anatase peaks are obtained at 2 $\theta$  of 26.7° (101), 38.4° (112), and 55.1° (211) planes of reflections (JCPDS card No. 01-071-1166). The TiO<sub>2</sub>'s rutile phase is observed with 2 $\theta$  values of 41.4° (110) (JCPDS card

No. 00-001-1292). Similarly, brookite peaks of TiO<sub>2</sub> are observed at 2 $\theta$  of 60.5° (600), 64.18° (023), and 66.23° (232) planes (JCPDS card No. 00-002-0514).

EDX spectrum as shown in Figure-1(b) elucidates that the synthesized ZTiO catalyst comprises of Ti, Zn, and O only. No other remarkable impurities were observed which reveals the purity of these nanoparticles. Spectral details are as listed in Table-1.

**Table-1:** Elemental composition of ZTiO NPs synthesized under optimum conditions.

Element	Weight%	Atomic%
Zn	25.35	11.34
Ti	40.45	25.21
O	33.40	62.54

**Surface morphology study:** FESEM images as shown in Figure-2 reveal the role of the surfactant in changing the morphology of the NPs from less organized to more regular structures which act as better photocatalysts. The morphology is complete with extensive voids and pores which is probably due to the escape of gases during calcination. Interlinked crystallites together form networked structure having irregular pore sizes.

TEM images confirm almost spherical particles with non-uniform thickness accompanied by interactive mixing of ZnO and TiO<sub>2</sub> particles crucial for photocatalytic efficiency. Well embedded particles attached to one another are seen in Figure-3. which is favourable for high degree of photocatalysis. The average size of a primary particle is observed to be 25 nm.

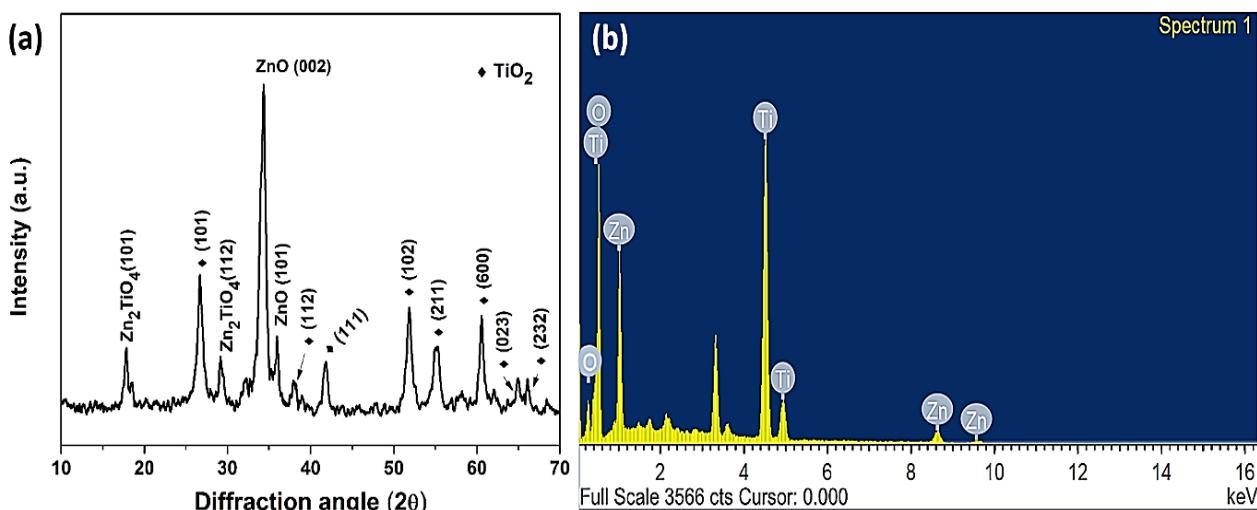


**Figure-1:** (a)XRD pattern (b) EDX spectra of ZTiO synthesised using SDS as additive and calcined at 650°C.

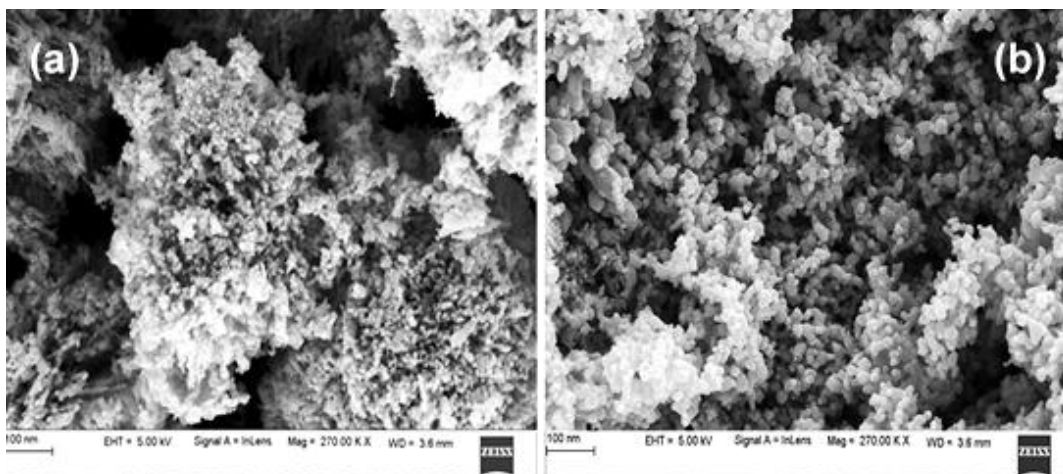


**Figure-2:** FESEM images of the electrochemically synthesized ZTiO nanoparticles a) in absence of surfactants b) in presence of SDS as additive.

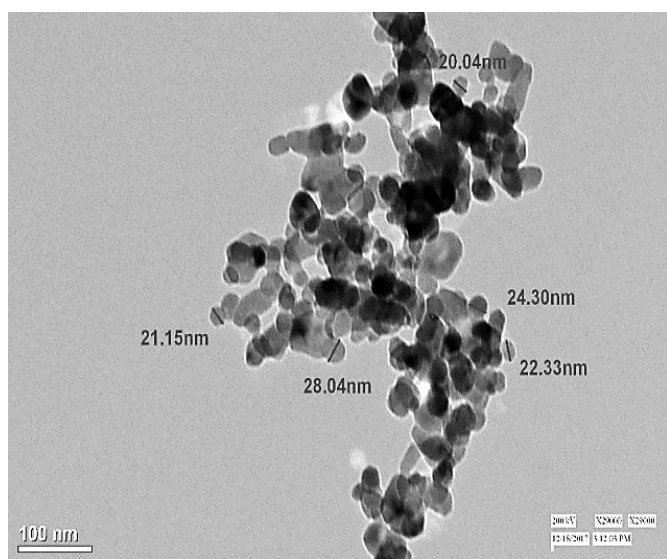


**Figure-3:** TEM image of ZTiO calcined at 650°C synthesized using SDS as additive.

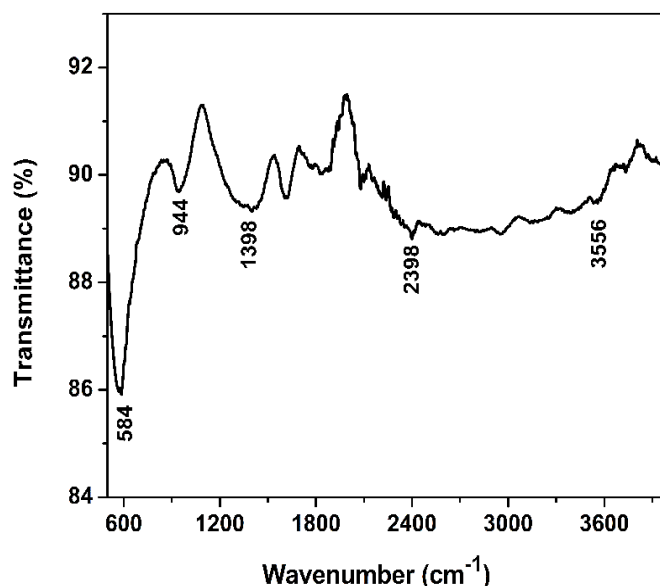


**Figure-4:** FTIR spectra of ZTiO calcined at 650°C synthesized using SDS as additive.

**FTIR spectra:** The FTIR spectrum is as shown in Figure-4. Due to inter-atomic vibrations generally, metal oxide particles give typical absorption bands less than  $1000\text{ cm}^{-1}$  i.e. in their fingerprint region. The spectrum of ZTiO displays wide absorption peaks ranging between  $3100\text{--}3700\text{ cm}^{-1}$  which correspond to the O-H (hydroxyl) stretching vibrations of water molecules adsorbed on the NP surface.<sup>25</sup> The peaks at  $944\text{ cm}^{-1}$  and  $584\text{ cm}^{-1}$  are the distinctive absorption peaks of Zn-O<sup>26</sup> and Ti-O<sup>27</sup> interatomic vibration. A wide absorption band at  $1398\text{ cm}^{-1}$  can be related to the vibrational modes for Ti-O and Ti-O-C bonds in the ZTiO nanocomposite<sup>28,29</sup>. The peak at  $2398\text{ cm}^{-1}$  is due to the Ti-O-Ti bond stretching in the nanocomposite.<sup>30</sup> This proves the formation of ZTiO composite. The functional groups play a substantial part in influencing photocatalysis since photocatalytic reactivity typically happens on the photocatalyst surface.

**Thermal Stability Assessment:** Thermogravimetric analysis reveals weight loss of 1.797% is observed at  $900^\circ\text{C}$  as seen in Figure-5 which confirms the capacity of the nanoparticles to resist heat. Micro voids may be the cause for weight loss over  $900^\circ\text{C}$ . Water and  $\text{O}_2$  and get thermally desorbed from ZTiO surface which could also be another factor indicating the porosity of the nanopowder.

**Band Gap:** UV spectrogram of ZTiO is evident in Figure-6(b) and the Band gap, studied using Tauc plot as depicted in Figure-6(a). Band gap energy for the nanocomposite has clearly shifted closer to ZnO giving a value of 3.2 eV. This may be accredited to the development of various defect levels inside the forbidden energy band.

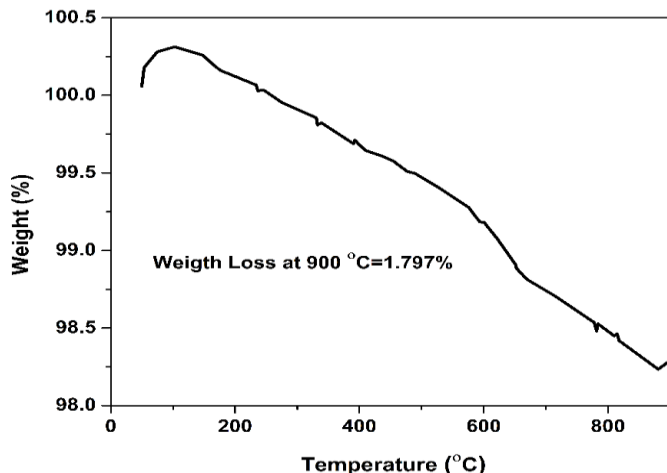


Figure-5: TGA of ZTiO nanoparticles synthesised at 650°C using SDS as additive.

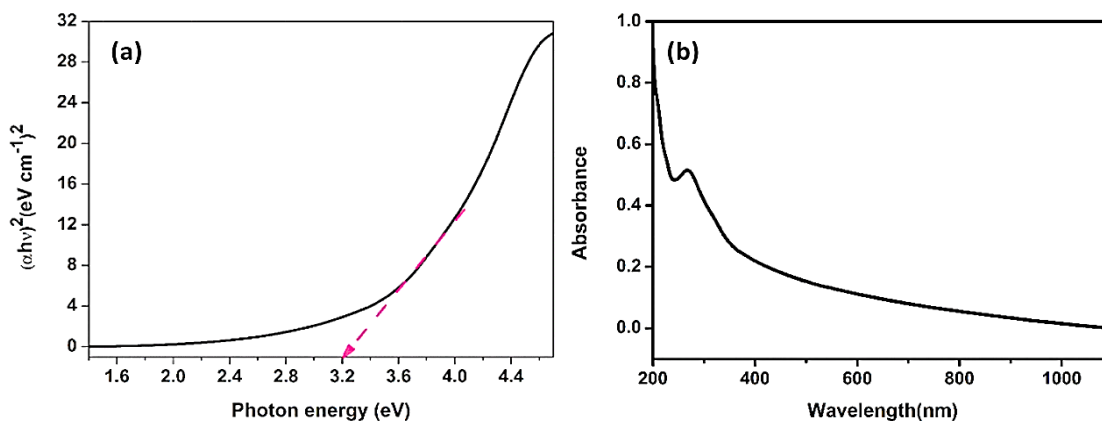


Figure-6: ZTiO nanoparticles (a) Tauc Plot (b) UV spectrogram for NPs calcined at 650°C synthesized using SDS as additive.

**Evaluation of photocatalytic activity:** Prior to photocatalysis, the suspension containing dye solutions along with ZTiO NPs were kept aside in the dark with continual stirring for 1 hour in order to establish an adsorption equilibrium. High decolourization efficiency of 93.6% and 91.75% for MB and EBT respectively was observed for ZTiO particles synthesized using SDS as additive as seen in Figure-9. The percentage of dye degradation accomplished by using ZTiO is determined with the help of the following formula,

$$\% \text{ of degradation} = \frac{C_i - C_f}{C_i} \times 100 \quad (2)$$

where  $C_i$  - initial concentration;  $C_f$  - final concentration of the dye.

**Effect of dye concentration:** The process of photodegradation is also dependant to some extent on the initial dye concentration taken. 5 ppm and 10 ppm solutions were easily degraded up to 95% for MB and 93% for EBT as seen in Figure-7. Whereas in 25ppm solution the percentage dropped to 75% and 52% which shows that 10ppm is the most suitable concentration to be degraded by the NPs.

**Reusability of the photocatalyst:** The synthesised NPs have been found to be useful as photocatalysts for three consecutive uses as seen in Figure-8. Degradation of 95.63%, 94.13%, 93.12% was seen for 10ppm MB and 93.70%, 92.52% and 91.31% degradation were achieved for 10ppm in the first, second and third cycle respectively. This clearly indicates that the NPs can be comfortably used even up to three times.

**Kinetics of dye degradation;** Estimation of the photocatalytic action of the synthesized ZTiO nanocomposites is done by the kinetics study for MB and EBT degradation. Photocatalysis is governed by the formula  $-\ln C/C_0 = kt$  where, dye concentration during time  $t$  is represented by  $C$  and initial concentration is represented by  $C_0$ .  $k$  stands for the rate constant in  $\text{min}^{-1}$ .<sup>31</sup>

The calculated rate constants are tabulated in Table-2. Degussa P25 commercial photocatalyst of  $\text{TiO}_2$  is taken as the reference under similar conditions. The table reveals that relatively high rate constant of  $0.017922\text{min}^{-1}$  and  $0.015767\text{min}^{-1}$  is obtained for ZTiO synthesized using SDS as an additive. The reason for greater activity is probably owing to the greater charge separation in the ZTiO nanocomposite. The electron-hole combination reduces giving greater photocatalytic behaviour.<sup>32</sup>

The kinetic plots for the degradation of MB and EBT SDS, PEG and Cetrimide is represented in Figure-9(a) and (b) synthesized without using surfactants and in the presence of respectively.

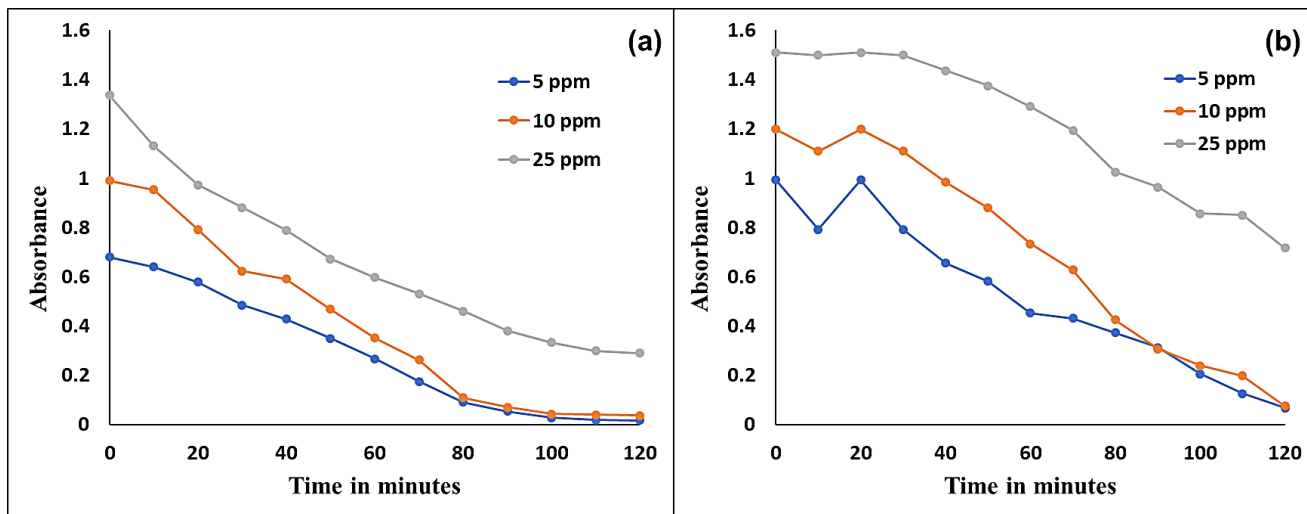


Figure-7: Photodegradation using ZnO-TiO<sub>2</sub> for varying concentrations of a) MB and b) EBT.

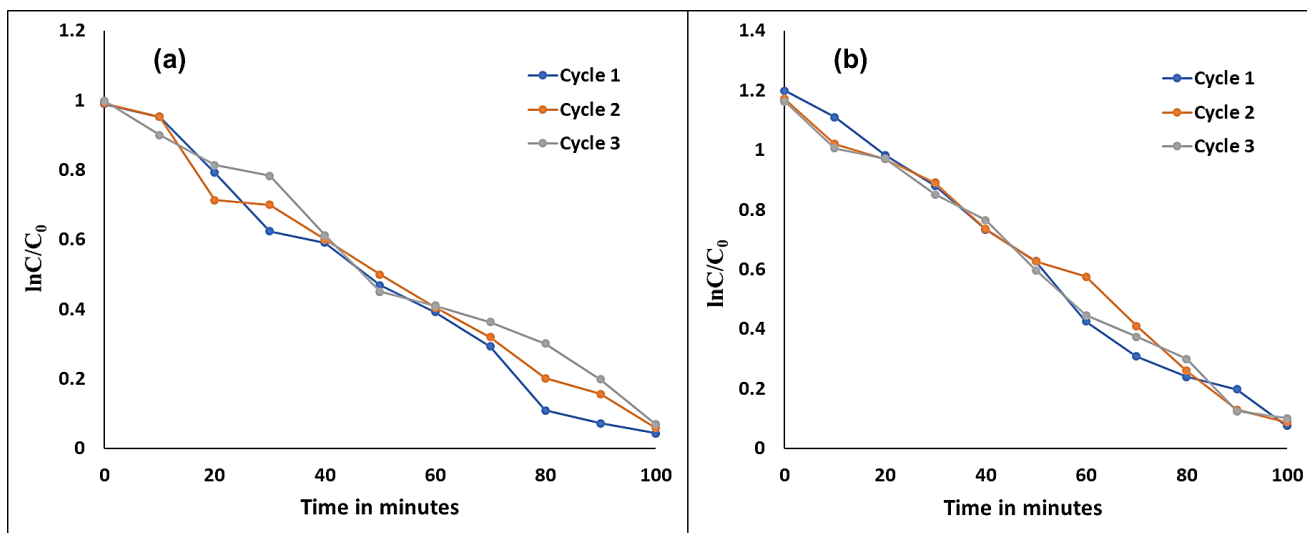


Figure-8: Reusability of the ZTiO photocatalysts for (a) MB and (b) EBT degradation.

Table-2: Kinetics parameters for the degradation of MB and EBT using different photocatalysts.

Photocatalyst	MB		EBT	
	% degradation	$k \times 10^{-2} \text{ min}^{-1}$	% degradation	$k \times 10^{-2} \text{ min}^{-1}$
ZTiO + No additive	90.9375	1.3369	85.4481	1.0014
ZTiO + SDS	95.6359	1.7922	93.7009	1.5767
ZTiO + PEG	92.5083	1.5045	89.0338	1.4658
ZTiO + Cetrimide	91.2977	1.3418	86.4798	1.0796
Degussa P25 TiO <sub>2</sub>	92.6856	1.3946	92.1655	1.5487

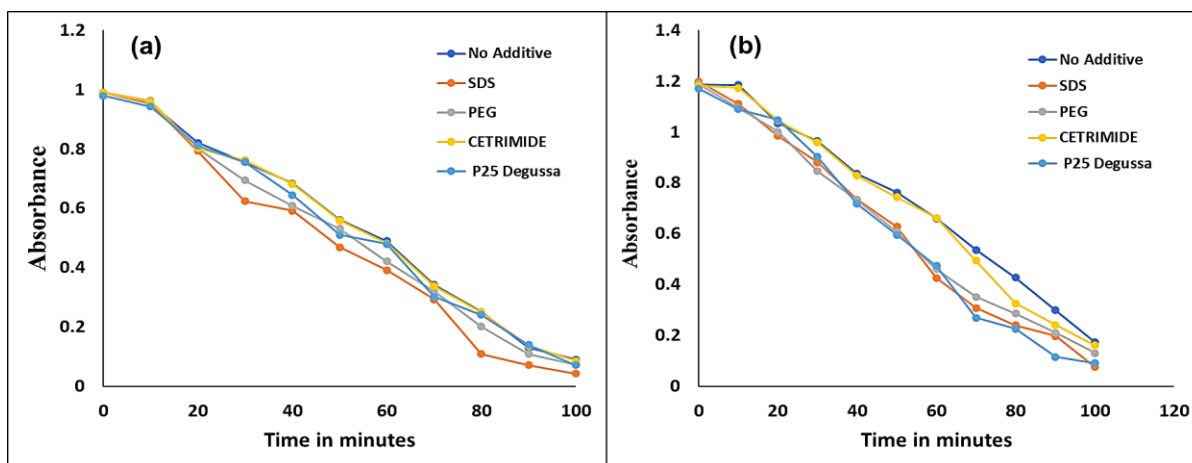


Figure-9: Photocatalytic degradation of (a) MB and (b) EBT.

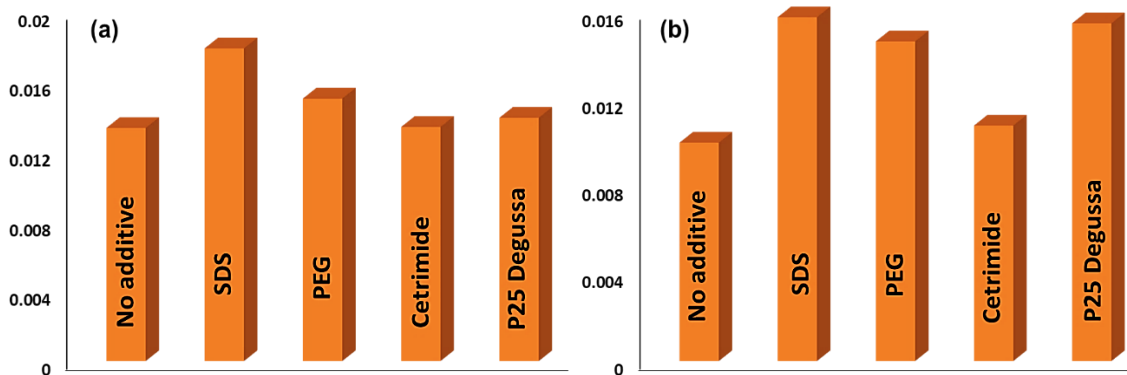
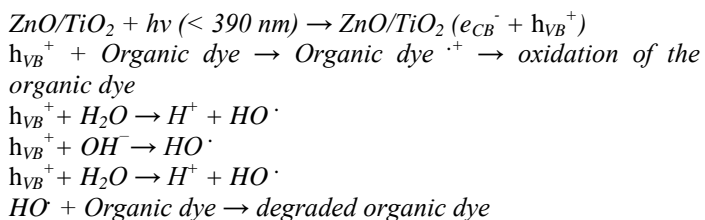


Figure-10: Kinetic studies of rate constant of the degradation of (a) MB (b) EBT with different photocatalysts.

Kinetic studies reveal that photodegradation follows pseudo first order kinetics. The rate constants  $k \text{ min}^{-1}$  are represented graphically in Figure-10(a) and (b) respectively.

TiO<sub>2</sub> behaves as the absorber owing to its absorption in the UV-Vis region. When ZTiO is irradiated with UV light, the large absorption gap of ZnO makes photoelectron-hole pairing difficult. Photogenerated electrons get transferred to ZnO's conduction band thus reducing the likelihood for photogenerated electron-hole pair recombination. This increases the number of existing active species. ZnO takes the role of the co-catalyst which traps electrons preventing additional recombination and enables photoelectrons to effortlessly trap dissolved radicals. Photoinduced holes trap OH<sup>-</sup> to give OH radicals which bring about dye degradation as shown in the mechanism<sup>33</sup>.



(where, h - hole, e<sup>-</sup> electron, VB- valence band and CB- conduction band)

**Evaluation of antibacterial activity:** Table-3 summarises the antimicrobial activity of the synthesised nanoparticles in terms of zone of inhibition. The results indicate that the ZTiO samples synthesized using SDS as an additive showed maximum antibacterial efficacy against all the microorganisms.

The bio-activity of the mixed metal oxide NPs can be credited to the abrasive texture of the synthesized ZTiONPs' surface which result in electrostatic forces binding ZTiO nanoparticles to the bacterial surface that eventually kills the bacteria<sup>34</sup>. Another reason could be the mechanical demolition of the bacterial cell membrane brought about by NP penetration. *P. aeruginosa* showed maximum resistance to the ZTiO nanoparticles as compared to the others. This could be attributed to the presence of a cytochrome oxidase in its cells accompanied by generation of extremely reactive species like OH<sup>·</sup>, H<sub>2</sub>O<sub>2</sub>, O<sub>2</sub><sup>2-</sup> on its surface<sup>35,36</sup>. Better results are observed with NPs synthesized in the presence of additives due to their smaller size and relatively greater surface area which triggers cytotoxicity towards the bacteria.

The zones of inhibition against the different bacteria are graphically represented in Figure-11. The graph shows that ZTiO nanoparticles synthesized in the presence of SDS show considerable increase in their antimicrobial ability compared to those synthesized in the absence of any surfactants. The role of the surfactant during the synthesis step to prevent agglomeration and give better dispersion of particles is evident from the improved antibacterial action.

**Evaluation of cytotoxic activity:** The toxic effects of NPs on target cells are explained in two different ways: i. Chemical toxicity grounded on its chemical composition due to release of toxic ions, surface catalyzed reactions of NPs or ROS formation. ii. Stress due to the surface, size and/or morphology of the NPs<sup>37</sup>.

Cytotoxicity induced by ZTiO nanoparticles synthesized using SDS as additive which showed appreciable results was tested by MTT assay on two cell lines-Cervical cancer cells HeLa and normal human embryonic kidney (Hek-293). The cytotoxic activity in the two cell lines used is as represented in Figure-13. The results disclose that synthesized ZTiONPs showed higher

cytotoxic effect on Hek cells as compared to HeLa cells. IC<sub>50</sub> value of 107.05µg/mL for Hek cells and IC<sub>50</sub> value of 132.6 µg/mL for HeLa cells were calculated from Figure-12. Interestingly, molecules exhibited decreased toxicity in Hek-293, the non-tumoral normal cell line. This invariably confirms that the molecules show increased toxicity towards the HeLa cancer cells. Literature reveals that NPs have the property of inducing cytotoxicity in a relatively cell specific manner which is also proliferation dependent. The cancer cells divide rapidly and are thus more susceptible in comparison to quiescent cells. Apoptosis in cancer cells can also be induced by nanoparticles. Apoptosis is characterized by the translocation of phospholipid phosphatidyl serine from within the plasma membrane to the cell's surface<sup>38</sup>. However, the IC<sub>50</sub> values of samples are comparatively higher than those reported for metal oxide nanoparticles<sup>39</sup> which indicates that the lower cytotoxicity makes the electrochemically synthesized nanoparticles relatively less toxic and hence almost biocompatible.

MTT results, as shown in Figure-13 prove that the cytotoxicity is dose and time dependent similar to that reported in the literature<sup>40</sup>.

**Table-3:** Zone of Inhibition for different bacteria.

Organism	Standard	Samples (Zone diameter in mm)			
	Streptomycin (10 mcg/disc) (mm)	ZTiO no additive (mm)	ZTiO+ SDS (mm)	ZTiO+ PEG (mm)	ZTiO + Cetrimide (mm)
<i>E. coli</i>	20	6	14	10	10
<i>K. pneumoniae</i>	12	6	14	10	10
<i>P. aeruginosa</i>	26	6	6	6	6
<i>S. aureus</i>	24	8	16	10	12

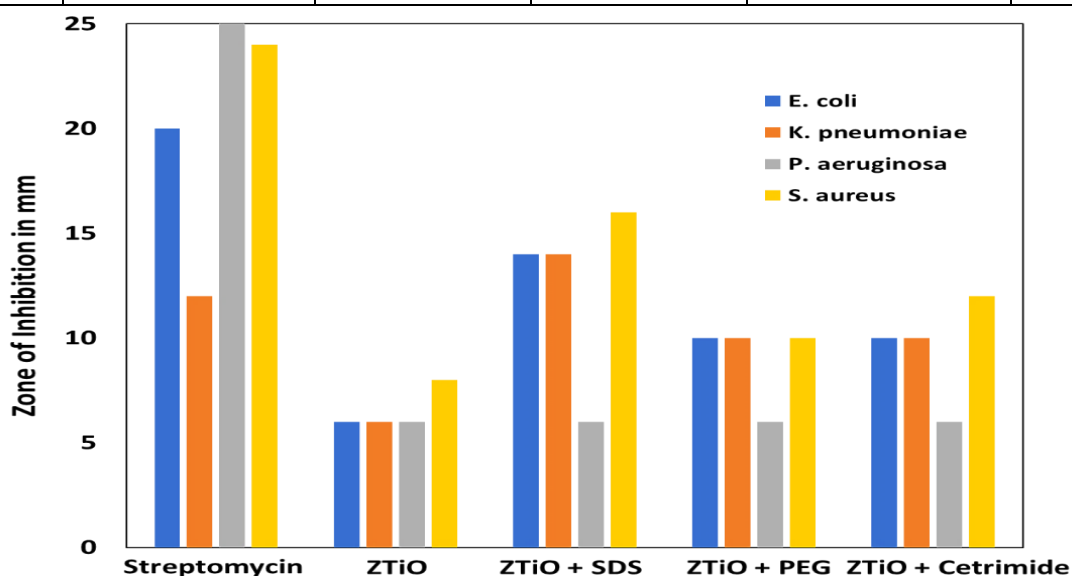


**Figure-11:** Antibacterial activity of the ZnO-TiO<sub>2</sub> NPs against *E. coli*, *K. pneumoniae*, *P. aeruginosa*, and *S. aureus*.

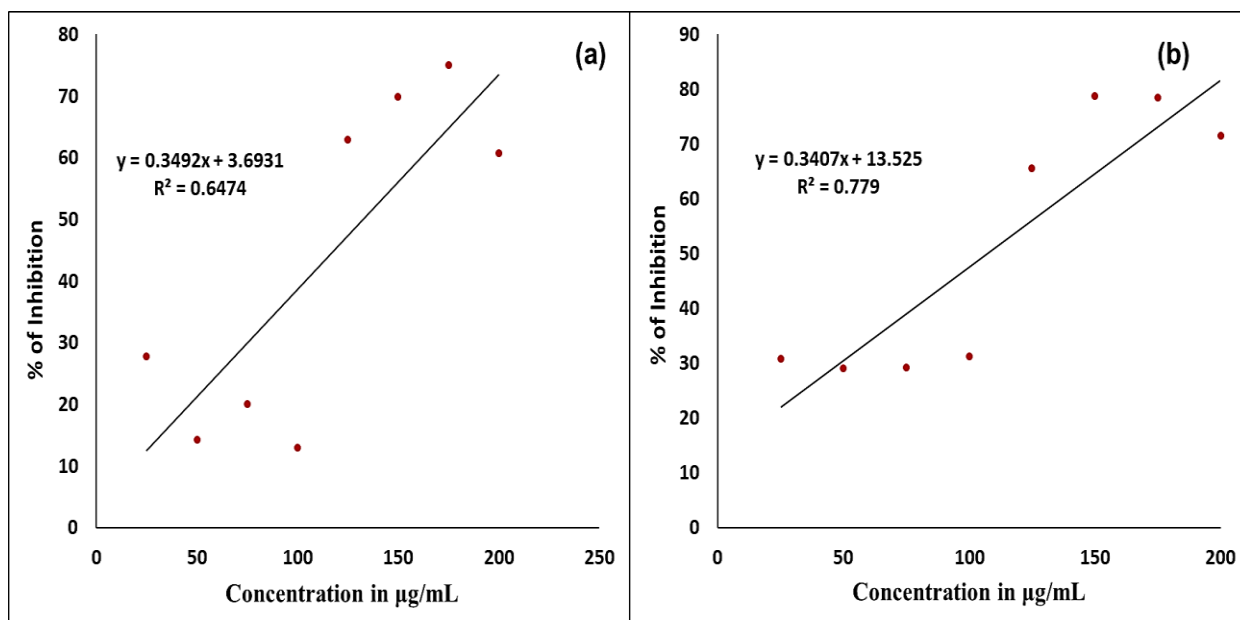


Figure-12: IC<sub>50</sub> calculation for (a) HeLa and (b) Hek cell lines.

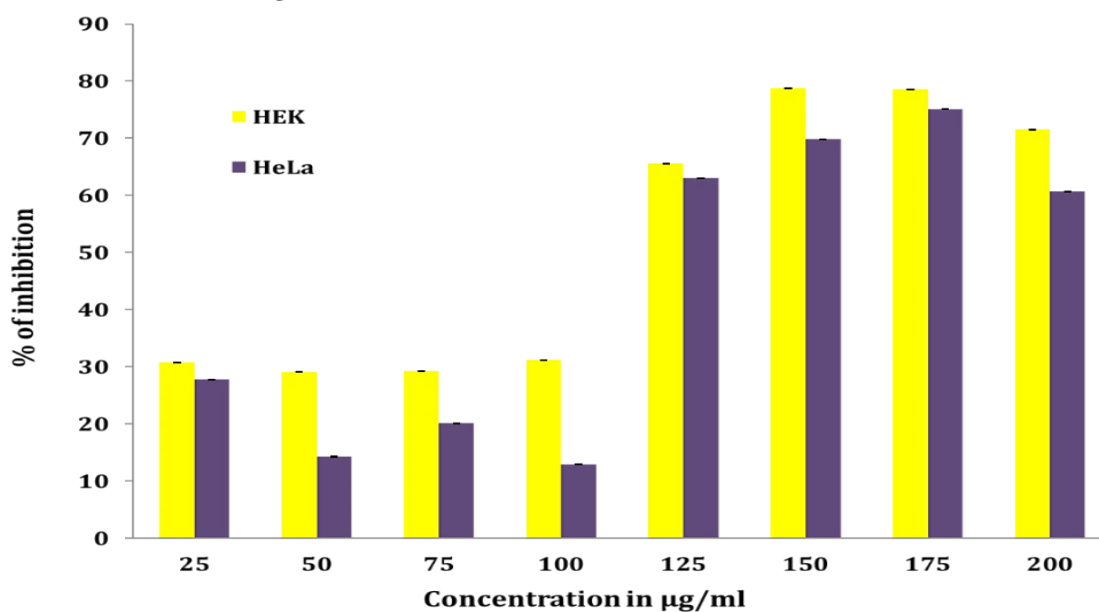


Figure-13: Cytotoxicity of ZTiO nanoparticles synthesized using SDS as additive on the proliferation of HeLa cancer cells and HeK cells.

**Evaluation of antioxidant Activity:** Antioxidant activity was analysed by assessing free radical scavenging activity (RSA) of the synthesized ZTiONPs and presented in Figure-14. The result reveals that RSA of the synthesized ZTiO was maximum for ZTiO particles synthesized in the presence of SDS as additive at the same concentration.

The results disclose substantial RSA ( $p \leq 0.05$ ) in the ZTiO NPs from 0% up to 55.43% along with its IC<sub>50</sub> value of 95.09 µg mL<sup>-1</sup>. Ascorbic acid was used as the positive control showing 75% inhibition at 50 µg mL<sup>-1</sup>.

DPPH molecule possesses a  $\pi$  system in addition to an unpaired electron on nitrogen. Molar absorptivity increases with substitution in the aromatic ring that extends conjugation and shifting its absorption bands towards longer wavelength. It gives a peak at 517 nm which is due to  $n \rightarrow \pi^*$  transition<sup>41</sup>. The DPPH solution which is deep violet progressively transitions to pale yellow in the presence of ZTiONPs due to free radical scavenging capacity. ZTiO shows a scavenging capacity of up to 70% in 90min. Antioxidant ability of ZTiONPs can be attributed to the transference of the electron density positioned on oxygen to nitrogen's odd electron of DPPH<sup>42</sup>.

ZTiO nanoparticles were also studied for their free radical scavenging activity by reducing power assay using nitric oxide RSA as shown in Figure-15. NPs exhibited different levels of antioxidant capacity. ZTiO synthesized in the presence of different additives showed almost similar free radical scavenging activity, however, the best results were seen for

those NPs synthesised in the presence of SDS. Many researchers have reported that antioxidant activity is closely related to the reducing power<sup>43</sup>. ZTiO NPs' reducing power is probably due to the existence of reductions possessing the ability to block free radicals and prevent peroxide formation<sup>44</sup>.

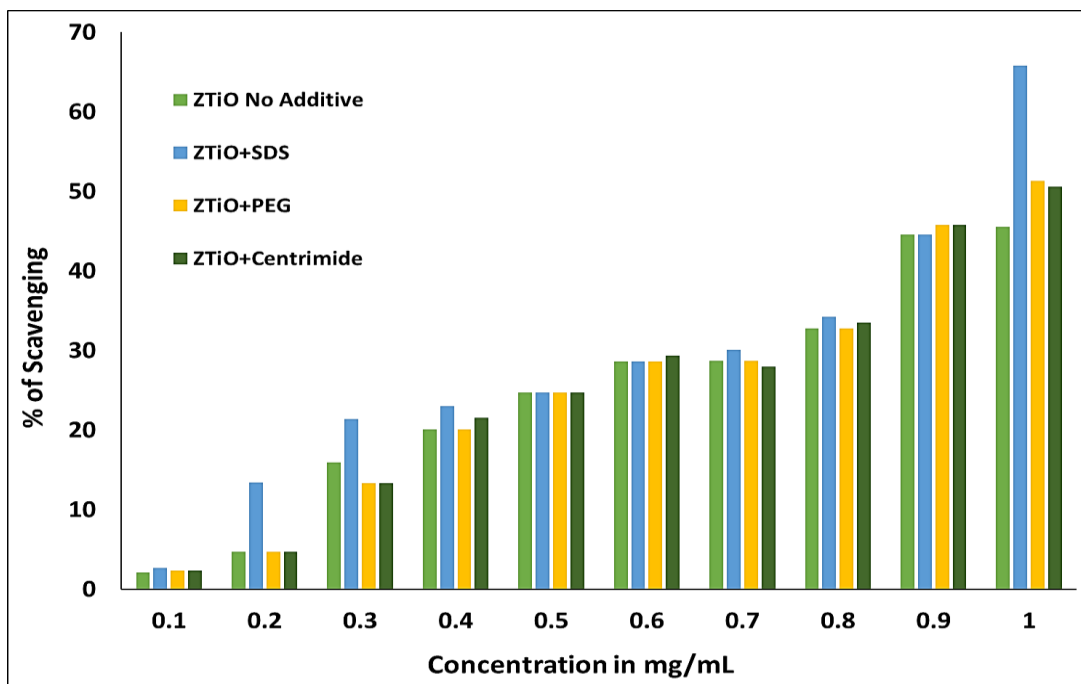


Figure-14: Free radical scavenging activity of ZTiO synthesized nanoparticles by DPPH method.

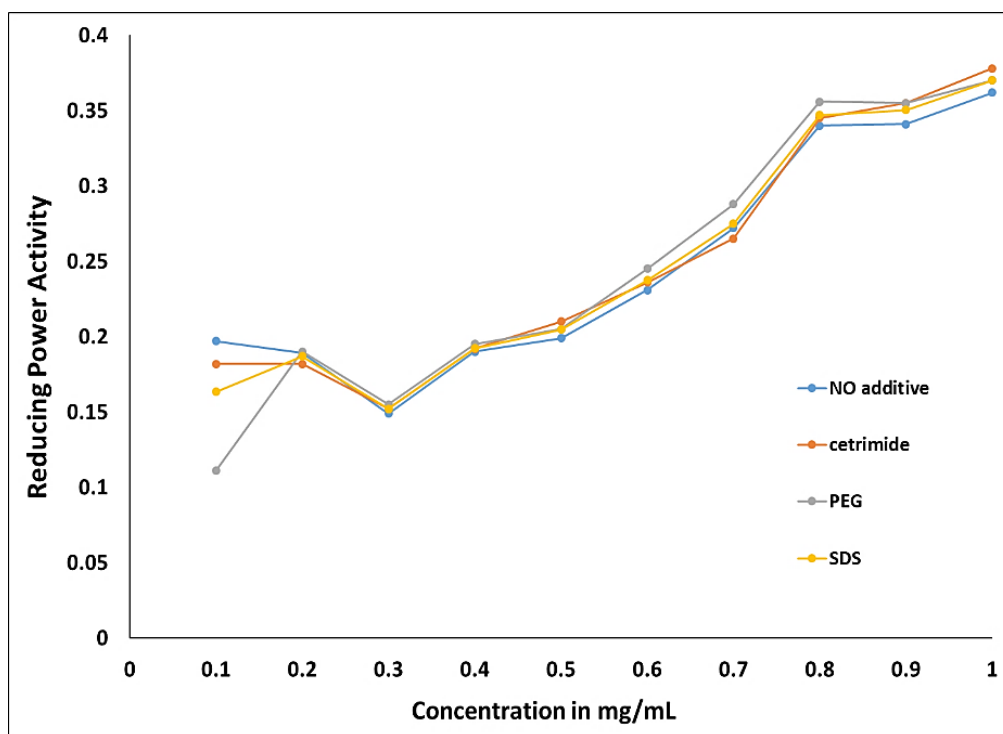


Figure-15: Reducing Power of the synthesised ZTiO nanoparticles.

## Conclusion

An efficient photocatalyst ZTiO was found to be synthesized using SDS as an additive by the electrochemical-thermal method synthesized at 650°C. These mixed oxide nanoparticles could bring about the successful photocatalytic decomposition of MB and EBT. TiO<sub>2</sub> behaves as the absorber of light energy and ZnO acts as its co-catalyst which reduces the electron-hole recombination. The mixed metal oxide can be reused effectively. Their effectiveness remains almost the same till three cycles and then decreases. These particles also show antimicrobial, antioxidant and cytotoxic properties which is revealed by the zone of inhibition, DPPH radical scavenging along with reducing power assay and IC<sub>50</sub> values respectively. However, these nanoparticles are relatively biocompatible as revealed by their high IC<sub>50</sub> values. Within the limits of the present study, the results suggest enhanced bioactivity and photocatalytic behaviour of ZTiO nanoparticles prepared using SDS as an additive. Hence, this study has been successful in demonstrating a convenient and cost-effective technique via electrochemical-thermal path for synthesis of large quantity of ZTiO nanoparticles which could be employed conveniently as photocatalysts and as plausible solutions to various biological problems.

## Acknowledgements

The authors are grateful to St. Aloysius College (Autonomous), Mangalore and Department of Biochemistry, College of Fisheries, Mangalore, for the laboratory facility to conduct this study.

## References

1. Royston, E., Ghosh, A., Kofinas, P., Harris, M.T. and Culver, J.N. (2008). Self-assembly of virus-structured high surface area nanomaterials and their application as battery electrodes. *Langmuir*, 24(3), 906-912.
2. Zheng, Y., Zheng, L., Zhan, Y., Lin, X., Zheng, Q. and Wei, K. (2007). Ag/ZnO heterostructure nanocrystals: synthesis, characterization, and photocatalysis. *Inorg. Chem.*, 46(17), 6980-6986.
3. Colón, G., Hidalgo, M., Navío, J.A., Melián, E.P., Díaz, O.G. and Dona, J. (2008). Influence of amine template on the photoactivity of TiO<sub>2</sub> nanoparticles obtained by hydrothermal treatment. *Appl. Catal. B: Environmental*, 78(1-2), 176-182.
4. Kim, H.G., Borse, P.H., Choi, W. and Lee, J.S. (2005). Photocatalytic nanodiodes for visible light photocatalysis. *Angew. Chem. Int. Ed.*, 44(29), 4585-4589.
5. Marci, G., Augugliaro, V., Lopez-Munoz, M. J., Martin, C., Palmisano, L., Rives, V., ... & Venezia, A. M. (2001). Preparation characterization and photocatalytic activity of polycrystalline ZnO/TiO<sub>2</sub> systems. 2. surface, bulk characterization, and 4-nitrophenol photodegradation in liquid- solid regime. *The Journal of Physical Chemistry B*, 105(5), 1033-1040.
6. An, T.-Q., Peng, J.-M., Tian, Z.-J., Zhao, H.-Y., Li, N., Liu, Y.-M., Chen, J.-Z., Leng, C.-L., Sun, Y. and Chang, D. (2013). Pseudorabies virus variant in bartha-k61-vaccinated pigs, china, 2012. *Emerging Infect. Dis.*, 19(11),1749.
7. Carp, O., Huisman, C.L. and Reller, A. (2004). Photoinduced reactivity of titanium dioxide. *Prog. Solid State Chem.*, 32(1-2), 33-177.
8. Losito, I., Amorisco, A., Palmisano, F. and Zambonin, P. (2005). X-ray photoelectron spectroscopy characterization of composite TiO<sub>2</sub>-poly (vinylidene fluoride) films synthesised for applications in pesticide photocatalytic degradation. *Appl. Surf. Sci.*, 240(1-4),180-188.
9. Akpan, U. and Hameed, B. (2011). Photocatalytic degradation of 2, 4-dichlorophenoxyacetic acid by Ca-Ce-W-TiO<sub>2</sub> composite photocatalyst. *Chem. Eng. J.*, 173(2), 369-375.
10. Naimi-Joubani, M., Shirzad-Siboni, M., Yang, J.-K., Gholami, M. and Farzadkia, M. (2015). Photocatalytic reduction of hexavalent chromium with illuminated ZnO/TiO<sub>2</sub> composite. *J. Ind. Eng. Chem.*, 22, 317-323.
11. Tom, R.T., Suryanarayanan, V., Reddy, P.G., Baskaran, S. and Pradeep, T. (2004). Ciprofloxacin-protected gold nanoparticles. *Langmuir*, 20(5),1909-1914.
12. Concannon, S.P., Crowe, T., Abercrombie, J., Molina, C., Hou, P., Sukumaran, D., Raj, P. and Leung, K.-P. (2003). Susceptibility of oral bacteria to an antimicrobial decapeptide. *J. Med. Microbiol.*, 52,1083-1093.
13. Sirelkhatim, A., Mahmud, S., Seeni, A., Kaus, N.H.M., Ann, L.C., Bakhori, S.K.M., Hasan, H. and Mohamad, D. (2015). Review on zinc oxide nanoparticles: antibacterial activity and toxicity mechanism. *Nano-Micro Lett.*, 7(3), 219-242.
14. Shalaby, A., Dimitriev, Y., Iordanova, R., Bachvarova-Nedelcheva, A. and Iliev, T. (2011). Modified sol-gel synthesis of submicron powders in the system ZnO-TiO<sub>2</sub>. *Journal of the University of Chemical Technology and Metallurgy*, 46(2),137-142.
15. Mandal, G. and Ganguly, T. (2011). Applications of nanomaterials in the different fields of photosciences. *Indian J. phys.*, 85(8),1229.
16. Reddy, V.R., Manjunath, V., Janardhanam, V., Kil, Y.-H. and Choi, C.-J. (2014). Electrical properties and current transport mechanisms of the Au/n-GaN Schottky structure with solution-processed high-k BaTiO<sub>3</sub> interlayer. *J. Electron. Mater.*, 43(9), 3499-3507.
17. Chandrappa, K.G., Venkatesha, T.V., Vathsala, K. and Shivakumara, C. (2010). A hybrid electrochemical-thermal

- method for the preparation of large ZnO nanoparticles. *Sci. Technol.*, 12(7), 2667-2678.
18. Li, Y., Li, X., Li, J. and Yin, J. (2006). Photocatalytic degradation of methyl orange by TiO<sub>2</sub>-coated activated carbon and kinetic study. *Water Res.*, 40(6), 1119-1126.
  19. Brand-Williams, W., Cuvelier, M.-E. and Berset, C. (1995). Use of a free radical method to evaluate antioxidant activity. *LWT-Food Sci. Technol.*, 28(1), 25-30.
  20. Poojary, M.M. and Passamonti, P. (2015). Optimization of extraction of high purity all-trans-lycopene from tomato pulp waste. *Food Chem.*, 188, 84-91.
  21. Pathan, A.H., Ramesh, A.K., Bakale, R.P., Naik, G.N., Kumar, H.R., Frampton, C.S., Rao, G.M.A. and Gudasi, K.B. (2015). Association of late transition metal complexes with ethyl 2-(2-(4-chlorophenylcarbamothioyl) hydrazono) propanoate: Design, synthesis and in vitro anticancer studies. *Inorganica Chimica Acta*, 430, 216-224.
  22. Hossain, M., Samad, M., Khan, M.D., Ara, N. and Islam, T. (2018). Study of ZnO-TiO<sub>2</sub> Composite Photocatalyst Mediated Photodegradation of Eosin Yellow. *IOSR J. Environ. Sci., Toxicol. Food Technol.*, 12, 58-67.
  23. Thamaphat, K., Limsuwan, P. and Ngotawornchai, B. (2008). Phase characterization of TiO<sub>2</sub> powder by XRD and TEM. *Kasetsart J.(Nat. Sci.)*, 42(5), 357-361.
  24. Ayed, S., Belgacem, R.B., Zayani, J.O. and Matoussi, A. (2016). Structural and optical properties of ZnO/TiO<sub>2</sub> composites. *Superlattices Microstruct.*, 91,118-128.
  25. Hussein, A.M., Iefanova, A.V., Koodali, R.T., Logue, B.A. and Shende, R.V. (2018). Interconnected ZnO2 doped ZnO/TiO<sub>2</sub> network photoanode for dye-sensitized solar cells. *Energy Rep.*, 4, 56-64.
  26. Khan, M., Naqvi, A.H. and Ahmad, M. (2015). Comparative study of the cytotoxic and genotoxic potentials of zinc oxide and titanium dioxide nanoparticles. *Toxicol. Rep.*, 2, 765-774.
  27. Ullah, H., Khan, K.A. and Khan, W.U. (2014). ZnO/TiO<sub>2</sub> nanocomposite synthesized by sol gel from highly soluble single source molecular precursor. *Chin. J. Chem. I Phy.*, 27, 548-554.
  28. Soni, B., Deshpande, M., Bhatt, S., Garg, N. and Chaki, S. (2013). Studies on ZnO nanorods synthesized by hydrothermal method and their characterization. *J. Nano-Electron. Phys.*, 5,4(2), 04077-6.
  29. Moradi, S., Aberoomand Azar, P., Raeis Farshid, S., Abedini Khorrami, S. and Givianrad, M.H. (2012). Effect of Additives on Characterization and Photocatalytic Activity of TiO<sub>2</sub>/ZnO Nanocomposite Prepared via Sol-Gel Process. *Int. J. Chem. Eng.*, 1-5.
  30. Stoyanova, A., Hitkova, H., Bachvarova-Nedelcheva, A., Iordanova, R., Ivanova, N. and Sredkova, M. (2013). Synthesis and antibacterial activity of TiO<sub>2</sub>/ZnO nanocomposites prepared via nonhydrolytic route. *J. Chem. Technol. Metall.*, 48(2), 154-161.
  31. Yin, R., Luo, Q., Wang, D., Sun, H., Li, Y., Li, X. and An, J. (2014). SnO<sub>2</sub>/gC<sub>3</sub>N<sub>4</sub> photocatalyst with enhanced visible-light photocatalytic activity. *J. Mater. Sci.*, 49(17), 6067-6073.
  32. Adhikari, S., Sarkar, D. and Madras, G. (2015). Highly efficient WO<sub>3</sub>-ZnO mixed oxides for photocatalysis. *RSC Adv.*, 5(16), 11895-11904.
  33. Gholami, M., Shirzad-Siboni, M., Farzadkia, M. and Yang, J.-K. (2016). Synthesis, characterization, and application of ZnO/TiO<sub>2</sub> nanocomposite for photocatalysis of a herbicide (Bentazon). *Desalin. Water Treat.*, 57(29), 13632-13644.
  34. Stoimenov, P.K., Klinger, R.L., Marchin, G.L. and Klabunde, K.J. (2002). Metal oxide nanoparticles as bactericidal agents. *Langmuir*, 18(17), 6679-6686.
  35. Yang, H., Liu, C., Yang, D., Zhang, H. and Xi, Z. (2009). Comparative study of cytotoxicity, oxidative stress and genotoxicity induced by four typical nanomaterials: the role of particle size, shape and composition. *J. Appl. Toxicol.*, 29(1), 69-78.
  36. Brayner, R., Ferrari-Iliou, R., Brivois, N., Djediat, S., Benedetti, M.F. and Fiévet, F. (2006). Toxicological impact studies based on Escherichia coli bacteria in ultrafine ZnO nanoparticles colloidal medium. *Nano lett.*, 6(4), 866-870.
  37. Clapp, A.R., Medintz, I.L., Mauro, J.M., Fisher, B.R., Bawendi, M.G. and Mattoussi, H. (2004). Fluorescence Resonance Energy Transfer Between Quantum Dot Donors and Dye-Labeled Protein Acceptors. *J. Am. Chem. Soc.*, 126(1), 301-310.
  38. Premanathan, M., Karthikeyan, K., Jeyasubramanian, K. and Manivannan, G. (2011). Selective toxicity of ZnO nanoparticles toward Gram-positive bacteria and cancer cells by apoptosis through lipid peroxidation. *Nanomed-Nanotechnol.*, 7(2), 184-192.
  39. Kim, I.-S., Baek, M. and Choi, S.-J. (2010). Comparative Cytotoxicity of Al<sub>2</sub>O<sub>3</sub>, CeO<sub>2</sub>, TiO<sub>2</sub> and ZnO Nanoparticles to Human Lung Cells. *J. Nanosci. Nanotechnol.*, 10(5), 3453-3458.
  40. Gies, V. and Zou, S. (2018). Systematic toxicity investigation of graphene oxide: evaluation of assay selection, cell type, exposure period and flake size. *Toxicol. Res.*, 7(1), 93-101.
  41. Das, D., Nath, B. C., Phukon, P., & Dolui, S. K. (2013). Synthesis of ZnO nanoparticles and evaluation of antioxidant and cytotoxic activity. *Colloids and Surfaces B: Biointerfaces*, 111, 556-560.
  42. Singh, B.N., Rawat, A.K.S., Khan, W., Naqvi, A.H. and Singh, B.R. (2014). Biosynthesis of stable antioxidant ZnO

- nanoparticles by *Pseudomonas aeruginosa* rhamnolipids. *PLoS One*, 9(9), e106937.
43. Ho, D.D., Neumann, A.U., Perelson, A.S., Chen, W., Leonard, J.M. and Markowitz, M. (1995). Rapid turnover of plasma virions and CD4 lymphocytes in HIV-1 infection. *Nature*, 373(6510), 123-126.
44. Singh, N. and Rajini, P. (2004). Free radical scavenging activity of an aqueous extract of potato peel. *Food Chem.*, 85(4), 611-616.